On the Radiative Properties of Cirrus in the Window Region and Their Influence on Remote Sensing of the Atmosphere[1]

KUO-NAN LIOU

Dept. of Atmospheric Sciences, University of Washington, Seattle 98195

(Manuscript received 1 August 1973, in revised form 30 October 1973)

ABSTRACT

Transmission, emission and reflection characteristics of cirrus clouds in the 800–1200 cm^{-1} window region are obtained by means of solving the transfer of infrared radiation in the realistic moist and dry model atmospheres. These model atmospheres include the water vapor within, above and below the cirrus clouds which are assumed to be composed of randomly oriented cylinders. Results of the radiation parameters are presented in terms of the geometrical thickness of cirrus as well as the model atmospheres. The discrepancies between the transmission and emission for flux and those for the vertically emergent intensity are pointed out and discussed. It is shown that the radiative properties of cirrus depend strongly upon the particle concentration. For a typical cirrus with a thickness of 1 km whose concentration is 0.05 cm^{-3}, the intensity transmission is about 0.65 with an emissivity of about 0.35. Further, based upon the theoretical analyses, the reductions in the effective temperature when cirrus clouds fill in the field of view of the radiometer reveal values from 0 to 60K. Having knowledge of the transmission and emission properties of cirrus clouds, it is demonstrated that the temperatures of the cloud and the underlying surface may be derived with reliable accuracy from meteorological satellites.

1. Introduction

One of the serious problems in the interpretation of radiometric measurements from orbiting meteorological satellites has been caused by the interference of clouds, particularly the globally distributed high cirrus whose radiative properties in the infrared region are mainly unknown. Attempts are made in this paper to derive the emission and transmission properties of cirrus in the atmospheric window region on the basis of solving the radiation transfer in model cloudy atmospheres. These model atmospheres consist not only of cloud particles, but also absorbing gases (primarily water vapor).

In this investigation, the window region is referred to the 800–1200 cm^{-1} spectral region which varies from one study to another. At these wavenumbers, absorption due to the atmospheric gases is comparatively small so that the blackbody surface temperature may be derived from the measured radiance. The effects of the imperfect transparency of a clear atmosphere have been described by Wark *et al.* (1962) and Sanders (1967). However, it has been noticed that the inference of the cloud top and the underlying surface temperature is greatly hampered when cirrus clouds fill in the field of view of the radiometer (Valovcin, 1968; Kuhn and Weickmann, 1969; Maul and Sidran, 1973). It is extremely important, therefore, to understand comprehensively the interaction of cirrus clouds with the radiation field in the atmosphere so that their influence on remote sensing may be carefully examined.

A three-layer model which is composed of the cirrus with water vapor above and below is constructed to evaluate the transfer of radiation within the atmosphere. The modeling of the composition of cirrus and the computation for their single scattering properties followed the author's previous studies (Liou, 1972b, 1973a). Moreover, a discrete-ordinate method for the transfer of a monochromatic radiation developed by Liou (1973b) was also employed as a basis to formulate the radiative transfer through cloud layers in a spectral interval. The absorption parameters for water vapor in the window region were taken from the measured data of Roach and Goody (1958) with modification for use in calculating the transfer of radiation in a non-scattering molecular atmosphere. Temperature and water vapor profiles for the tropical and middle latitude winter atmospheres tabulated by McClatchey *et al.* (1971) were chosen in the computations to represent wet and dry atmospheric conditions, respectively. The transmitted and reflected intensity and the transmission, reflection and emission for a number of cloud depths are presented and discussed. Some discussions are also made on the role of cirrus on remote sensing of the atmosphere.

2. Model atmospheres

A plane-parallel atmospheric model consisting of three layers (illustrated in Fig. 1) is employed to

[1] Contribution No. 300, Department of Atmospheric Sciences, University of Washington.

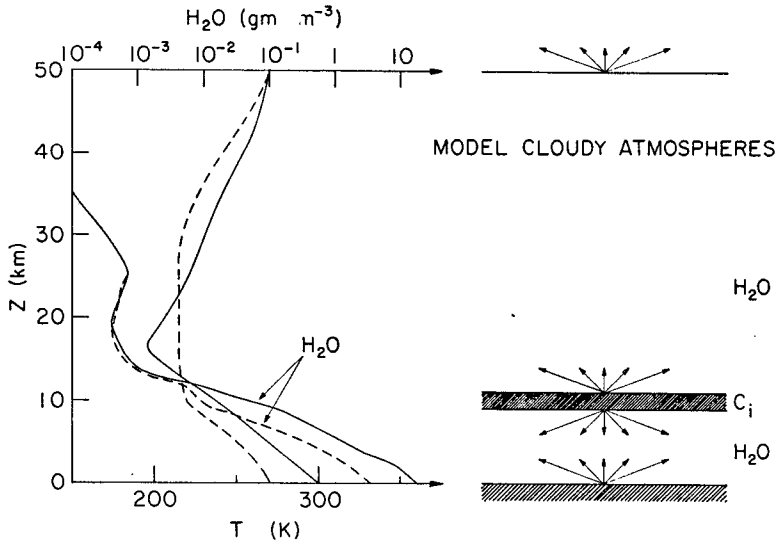

FIG. 1. Model cloudy atmospheres for radiative transfer computations. The solid lines on the left-hand side of the figure denote the temperature and water vapor height profiles for a tropical atmosphere, whereas the dashed lines represent those for a mid-latitude winter atmosphere.

evaluate the transfer of thermal infrared radiation. The temperature and water vapor profiles were taken from a moist and a dry atmosphere tabulated by McClatchey *et al.* (1971) for the tropics and mid-latitude winter conditions, respectively. These parameters were given at 1-km height intervals up to 25 km. Temperature and water vapor at two neighboring layers were averaged to obtain values for each interval so that the transmission functions and the emission contributions from water vapor could be calculated.

The base of cirrus clouds is assumed to be located at 8 km in the atmosphere where their thicknesses ΔZ may be changed up to 6 km. The isothermal temperature of cirrus is assumed to be the same as that of the environment at a height of 10 km. The effective water vapor content within the cirrus is estimated from the saturated vapor amount over pure ice at the assumed cloud temperature.

Based on the comprehensive observations of Weickmann (1949), cirrus contain mainly hexagonal columns whose lengths and radii are about 200 and 30 μm, respectively. The concentration generally varies from 0.1 to 1 cm^{-3}, while monodisperse properties of ice crystals were usually observed. In a recent investigation, Heymsfield and Knollenberg (1972) reported that cirrus generating cells are composed of primarily hexagonal columns having a mean crystal length of $\sim$600–1000 μm. The concentration was found to be $\sim$0.01–0.05 cm^{-3}. In order to perform the single scattering computations discussed in the following section, we assume that the ice cylinders are randomly oriented in space having circular cross sections with a mean length of 200 μm, a mean radius of 30 μm, and a mean concentration of 0.05 cm^{-3}. For comparison purposes, we also model a cirrus composed of spheres with a mode radius of 50 μm, the volume of which is "equivalent" to that of a 200μm, 30 μm cylinder.

3. Single scattering

The shapes, sizes, orientations, and the real and imaginary parts of the refractive indices of cloud particles are properties that are required in the single scattering computations. On the basis of these characteristics of cloud particles, three fundamental optical parameters can therefore be derived. These parameters are the phase function, the extinction cross section, and the single scattering albedo. The computations of these values were based on the author's previous theoretical investigations (Liou, 1972a,b,c) for scattering by cylindrical particles. Mie computations for polydisperse spheres (Liou and Hansen, 1971) having a mode radius of 50 μm were also carried out for the purposes of comparison. A modified gamma function for the size distribution is employed mainly to smooth out the fluctuation characteristics of scattering by a single particle. No attempts are made in this investigation to discuss the effects of size distributions on the scattered radiation. The real (n_r) and imaginary (n_i) parts of the refractive indices for ice in the 8–12 μm window region were taken from the table by Irvine and Pollack (1968) who interpolated the measured data to a 0.5-μm interval.

Table 1 lists the optical properties for randomly oriented ice cylinders and polydisperse ice spheres. In this table we find that the variation of the imaginary parts of the refractive indices from 8 to 11 μm are rather small. However, at 11.5 and 12 μm ice seems to possess

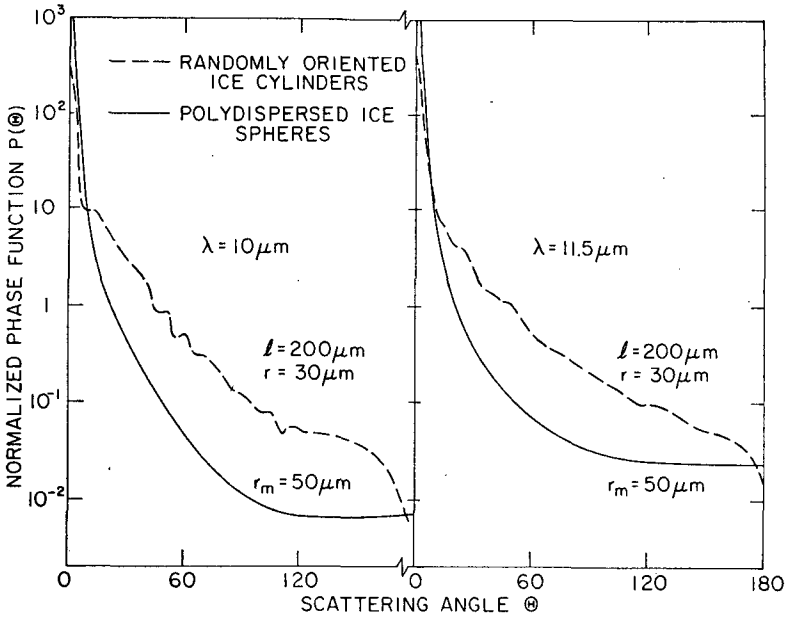

FIG. 2. Phase functions for randomly oriented ice cylinders (dashed lines) and ice spheres (solid lines) at incident wavelengths of 10 and 11.5 μm.

larger absorption properties as compared to the previous wavelengths. Values of the single scattering albedo $\tilde{\omega}_0$ are tabulated for both randomly oriented cylinders and polydisperse spheres. The differences due to the shape factor appear to be small, but noticeable. The extinction cross sections are calculated based on a particle concentration of 0.05 cm^{-3}. The values for cylindrical particles are clearly greater than those for spheres in which the two kinds of particles have about the same volume (and therefore the same mass). We note that it is based on the extinction cross section that the optical depth of a cloud is derived. Thus, from these comparisons, it is obvious that the optical depth of a cloud would be underestimated by a factor of about 1.5 if the assumption of an equivalent sphere is employed. We may increase the radii for spheres so that larger extinction cross sections could be obtained to match those of the cylinders. However, larger spheres would absorb more incident radiation and hence decrease the values of the single scattering albedo.

TABLE 1. Optical properties* for randomly oriented ice cylinders (length 200 μm, radius 30 μm) and polydisperse spheres (radius 50 μm) in the 8–12 μm window region for a particle number density of 0.05 cm^{-3}.

λ (μm)	n_r	n_i	Cylinders $\tilde{\omega}_0$	Cylinders β_e (km^{-1})	Spheres $\tilde{\omega}_0$	Spheres β_e (km^{-1})
8.0	1.219	0.0369	0.543	1.391	0.510	0.906
8.5	1.217	0.0352	0.554	1.486	0.511	0.909
9.0	1.210	0.0365	0.546	1.385	0.510	0.912
9.5	1.192	0.0310	0.527	1.344	0.517	0.917
10.0	1.152	0.0413	0.520	1.387	0.507	0.917
10.5	1.195	0.0602	0.495	1.374	0.499	0.916
11.0	1.290	0.0945	0.516	1.367	0.506	0.917
11.5	1.393	0.1140	0.545	1.345	0.514	0.921
12.0	1.480	0.1200	0.567	1.478	0.521	0.924

* In the original manuscript, the imaginary parts of the refractive indices n_i for ice at wavelengths of 11.5 and 12 μm were taken from the table provided by Irvine and Pollack (1968, pp. 332–333). It appears that the data should be a factor of 10 larger. We have redone the computations employing the values given in Table 1 now. It was found that the changes in results presented in Figs. 3–7 were no more than 0.05%. More recent measurements obtained by Bertie *et al.* (1969) and Schaaf and Williams (1973) indicated that n_i for ice at these wavelengths are larger than those previously reported. At 840 cm^{-1} (11.9 μm), Schaaf and Williams gave n_r=1.259, and n_i=0.409 for ice at −7C. The resulting $\tilde{\omega}_0$ and β_e are 0.531 and 1.454 km^{-1}, respectively, for cylinders. Values of these two parameters for other wavenumbers were also found to have insignificant variations as compared with those in Table 1. The reason that larger n_i's produce negligible variations for these two parmeters is because very large size parmeters are considered in the single scattering computations. Consequently, neither the Irvine and Pollacks errors nor the new measurements for the 12-μm absorption band would affect the discussion presented in this paper.

Since the wavelength regions of 8–11 μm and 11.5–12 μm apparently have similar optical properties as indicated in Table 1, we chose 10 and 11.5 μm to represent two groups in the computations of phase functions. Fig. 2 illustrates the phase functions for randomly oriented ice cylinders and polydisperse spheres with a mode radius of 50 μm. In our previous investigation, the theoretical results of the phase function for randomly oriented ice cylinders were compared with the laboratory scattering measurements for columns reported by Huffman and Thursby (1969). Comparisons reveal close agreement between theory and experiment. Moreover, we also found that visible and near-infrared radiation scattered by spheres concentrates much more in the forward and backward directions at the expense of the scattering at ~90°

scattering angle. As shown in Fig. 2, this conclusion is also applied to the IR wavelengths in the window region. If we increase the radii of spheres so as to obtain comparable extinction cross sections as those of cylinders, in addition to decreasing the single scattering albedo, we also change the scattering patterns for which spheres scatter tremendous radiation in the forward directions. Hence we conclude that neither equivalent mass nor equivalent cross section of spheres serves as a good approximation for evaluating the scattering properties of ice crystals. (In the Appendix, we tabulate the transmission and emission of cirrus based upon the assumptions of randomly oriented ice cylinders and equivalent cross section of spheres for the purpose of comparisons.) In Fig. 2, it is seen that owing to the large particle sizes all the scattering features are washed out for both 10 and 11.5 μm wavelengths. In the radiative transfer calculations, these two phase functions are used. Moreover, the wavelength dependences of optical properties are transferred to the wavenumber domain of 800–1200 cm^{-1} by interpolation in a 50 cm^{-1} spectral interval.

4. Radiative transfer in cirrus cloud layers

For a plane-parallel cloud layer which is in local thermodynamic equilibrium the appropriate transfer equation describing the infrared radiation field may be expressed as

$$\mu\frac{dI_\nu(\tau,\mu)}{d\tau}=I_\nu(\tau,\mu)-\frac{\tilde{\omega}_\nu}{2}\int_{-1}^{+1}p_\nu(\mu,\mu')I_\nu(\tau,\mu')d\mu' -(1-\tilde{\omega}_\nu)B_\nu[T(\tau)], \quad (1)$$

where I_ν represents the monochromatic intensity, τ the optical depth, μ the emergent angle with respect to the zenith, and T the cloud temperature. The axially symmetrical phase function can be expanded in Legendre polynomials consisting of a finite number of terms (Chandrasekhar, 1950)

$$p_\nu(\mu,\mu')=\frac{1}{2\pi}\int_{-1}^{+1}p_\nu(\mu,\phi;\mu',\phi')d\phi' \approx\sum_{l=0}^{N}\tilde{\omega}_{l,\nu}P_{l,\nu}(\mu)P_{l,\nu}(\mu'), \quad (2)$$

such that

$$\frac{1}{2}\int_{-1}^{+1}p_\nu(\cos\Theta)d\cos\Theta=\tilde{\omega}_{0,\nu}=1 \text{ for every } \nu. \quad (3)$$

The angle Θ in Eq. (3) denotes the scattering angle, i.e., the angle between the incident and scattered waves. The well-known single scattering albedo

$$\tilde{\omega}_\nu=\frac{\beta_{s,\nu}}{\beta_{s,\nu}+\beta_{a,\nu}+nk_\nu}, \quad (4)$$

where $\beta_{s,\nu}$ and $\beta_{a,\nu}$ denote the volume scattering and absorption cross sections for cloud particles of wavenumber ν, n is the number density of the absorbing gases within the cloud layer, and k_ν represents the absorption coefficient of the gases. The total optical thickness of a cloud layer may be obtained by multiplying the denominator in Eq .(4) by the thickness ΔZ. The Planck function expressed in the wavenumber domain is

$$B_\nu(T)=\frac{2hc^2\nu^3}{e^{hc\nu/KT}-1}. \quad (5)$$

In this equation h and K are known as Planck's and Boltzmann's constants, respectively, and c is the velocity of light.

The formal solution of Eq. (1) and the numerical techniques for solving it by employing a discrete-ordinate method have been comprehensively described by Liou (1973b). Hence we shall introduce only the necessary formulations for the convenience of discussions in this paper. We omit the frequency index ν on the phase function whose variations in a spectral interval may be neglected. Replacing the integration by summation according to the Gauss's quadrature formula, Eq. (1) becomes

$$\mu_i\frac{dI_\nu(\tau,\mu_i)}{d\tau}=I_\nu(\tau,\mu_i)-\frac{\tilde{\omega}_\nu}{2}\sum_{l=0}^{N}\tilde{\omega}_lP_l(\mu_i) \times\sum_j a_jP_l(\mu_j)I_\nu(\tau,\mu_j)-(1-\tilde{\omega}_\nu)B_\nu[T(\tau)]. \quad (6)$$

Here i and j are from $-n$ to n ($n\neq0$), a_j are the quadrature weights, and μ_i denote emergent angles at discrete-streams i. The complete solutions for the above differential equations assuming an isothermal cloud layer may be obtained by seeking a general solution for the homogeneous part plus adding a particular solution. The final form is

$$I_\nu(\tau,\mu_i)=\sum_j L_jW_{j,\nu}(\mu_i)\exp(-k_{j,\nu}\tau)+B_\nu(T_c), \quad (7)$$

where

$$W_{j,\nu}(\mu_i)=\frac{\tilde{\omega}_\nu}{1+\mu_ik_{j,\nu}}\sum_{l=0}^{N}\tilde{\omega}_l\xi_l(k_{j,\nu})P_l(\mu_i), \quad (8)$$

$$\xi_{l+1}=-\frac{2l+1-\tilde{\omega}_\nu\tilde{\omega}_l}{k_{j,\nu}(l+1)}\xi_l-\frac{l}{l+1}\xi_{l-1}. \quad (9)$$

In the above equations, $k_{j,\nu}$ are the eigensolutions of the differential equations at a given wavenumber, and L_j are proportional constants to be determined by the boundary conditions of radiation in a spectral interval discussed in the next section.

Since the equation of transfer describes only monochromatic radiation, we shall now average the derived

intensity over a spectral interval $\Delta\nu$ as

$$I_{\bar{\nu}}(\tau,\mu_i)=\sum_j L_j\int_{\Delta\nu} W_{j,\nu}(\mu_i)\exp(-k_{j,\nu}\tau)\frac{d\nu}{\Delta\nu}+B_{\bar{\nu}}(T_c), \quad (10)$$

where the bar over the wavenumber index denotes a spectral integration for any function F such that

$$F_{\bar{\nu}}=\frac{1}{\Delta\nu}\int_{\Delta\nu} F_\nu d\nu. \quad (11)$$

Hence, from the components of radiation in a spectral interval resulting from the emission and absorption due to the gases and the emission from the ground, we may obtain the coefficients L_j.

5. Radiative transfer in molecular atmospheres

a. Upward and downward intensity

For a non-scattering molecular atmosphere in local thermodynamic equilibrium, the transfer equation may be written

$$\mu\frac{dI_\nu(\tau,\mu)}{d\tau}=I_\nu(\tau,\mu)-B_\nu[T(\tau)]. \quad (12)$$

The implicit solutions for the downward and upward intensity at the top and base of a cloud layer, respectively, can be easily derived as

$$I_\nu\downarrow(\tau_t,-\mu_i)=\int_{\tau_t}^{\tau_\infty} B_\nu[T(\tau)]\exp[-(\tau-\tau_t)/\mu_i]\frac{d\tau}{\mu_i}, \quad (13)$$

$$I_\nu\uparrow(\tau_b,\mu_i)=B_\nu(T_g)\exp(-\tau_b/\mu_i)+\int_0^{\tau_b} B_\nu[T(\tau)]\exp[-(\tau_b-\tau)/\mu_i]\frac{d\tau}{\mu_i}, \quad (14)$$

where τ_b and τ_t denote the optical thicknesses from the earth surface to the base and top of a cloud layer respectively and T_g represents the ground temperature. In order to transform Eqs. (13) and (14) to the proper height coordinate Z, we denote the difference of two optical thicknesses as

$$\tau_2-\tau_1=\int_{Z_1}^{Z_2} k_\nu(Z)n(Z)dZ, \quad (15)$$

where $k_\nu(Z)$ and $n(Z)$ represent the absorption coefficient and the concentration, respectively, at a given height Z of absorbing gases.

By virtue of Eq. (15), Eqs. (13) and (14) yield the forms

$$I_\nu\downarrow(Z_t,-\mu_i)=\int_{Z_t}^{\infty} B_\nu[T(Z)]\frac{d}{dZ}\times\left\{\exp\left[-\frac{1}{\mu_i}\int_{Z_t}^{Z} k_\nu(Z)n(Z)dZ\right]\right\}dZ, \quad (16)$$

$$I_\nu\uparrow(Z_b,\mu_i)=B_\nu(T_g)\exp\left[-\frac{1}{\mu_i}\int_0^{Z_b} k_\nu(Z)n(Z)dZ\right]+\int_0^{Z_b} B_\nu[T(Z)]\frac{d}{dZ}\times\left\{\exp\left[-\frac{1}{\mu_i}\int_Z^{Z_b} k_\nu(Z)n(Z)dZ\right]\right\}dZ. \quad (17)$$

We further define a general expression for the transmission function, i.e.,

$$\tau_\nu(Z_2,Z_1;\mu_i)=\exp\left[-\frac{1}{\mu_i}\int_{Z_1}^{Z_2} k_\nu(Z)n(Z)dZ\right]. \quad (18)$$

Substituting Eq. (18) into the above equations, we have (we neglect the parameter μ_i in the argument for simplicity)

$$I_\nu\downarrow(Z_t,-\mu_i)=\int_1^{\tau_\nu(\infty,Z_t)} B_\nu[T(Z)]d\tau_\nu(Z,Z_t), \quad (19)$$

$$I_\nu\uparrow(Z_b,\mu_i)=B_\nu(T_g)\tau_\nu(Z_b,0)+\int_{\tau_\nu(Z_b,0)}^{1} B_\nu[T(Z)]d\tau_\nu(Z_b,Z). \quad (20)$$

b. Transmission function for water vapor in the window region

Roach and Goody (1958) measured the infrared absorption by water vapor in the 1232–778 cm^{-1} window region which was divided into seven spectral intervals. The absorption due to 9.6 μm ozone band was not considered. They explained this absorption by two different causes. One is due to the selective absorption by weak lines, while the other arises from the continuous absorption. The selective absorption is caused by single lines with a distance much larger than the half-width and can be described to a good approximation of Goody's (1964) statistical model with an exponential distribution of line intensities. The continuous absorption in the window region was discussed theoretically by Elsasser and Culbertson (1960) who pointed out that this continuum comes from the wings of very strong lines concentrated at the peak of the rotational band and the 6.3-μm vibration-rotational band. Consequently, the extinction of the continuum should follow Lambert's law. [Recently, McClatchey *et al.* (1973) indicated the *possible* existence of the water dimer (H_2O:H_2O) for the continuous absorption in the 8–14 μm region.]

So with these two sources of absorption taken into consideration, the transmission function at each spectral interval may be written

$$\tau_{\bar{\nu}}(u)=\tau_{\bar{\nu}}(\text{selective})\times\tau_{\bar{\nu}}(\text{continuum})=\exp\{-[\eta_\nu(u/\mu_i)^{\frac{1}{2}}+\beta_\nu u/\mu_i]\}, \quad (21)$$

where the vertical path length (gm cm^{-2})

$$u=\int_{Z_1}^{Z_2}\rho_w dZ, \tag{22}$$

and the parameter

$$\eta_\nu=(\pi\alpha\sigma)^{\frac{1}{2}}/\delta, \tag{23}$$

with ρ_w the water vapor density, σ the mean line intensity, δ the mean line spacing and α the mean line width. By fitting the mean transmission function such that

$$\tau_{\bar{\nu}}=\frac{1}{\Delta\nu}\int_{\Delta\nu}e^{-k_\nu u}d\nu\approx\frac{1}{I}\sum_{i=1}^{I}e^{-k_i u}, \tag{24}$$

an equivalent absorption coefficient may be obtained. The k_i may then be physically interpreted as mean absorption coefficients for each sub-spectral interval $\Delta\nu_i$. In this way, the transmission function and the single scattering albedo with contributions due to gases can be evaluated at desired spectral intervals. This technique has been previously used by Yamamoto *et al.* (1970) and Houghton and Hunt (1971).

Thus, with the given model atmospheric temperature and water vapor density profiles described in Section 2, the upward and downward intensities incident on the boundaries of clouds at each spectral interval can be evaluated by noting that

$$I_{\bar{\nu}}\downarrow(Z_t,-\mu_i)=\frac{1}{\Delta\nu}\int_{\Delta\nu}I_\nu\downarrow(Z_t,-\mu_i)d\nu, \tag{25}$$

$$I_{\bar{\nu}}\uparrow(Z_b,\mu_i)=\frac{1}{\Delta\nu}\int_{\Delta\nu}I_\nu\uparrow(Z_b,\mu_i)d\nu. \tag{26}$$

Finally, substituting (25) and (26) into (10), and denoting the optical depth of a cloud as τ_N, we obtain two sets of equations to determine the coefficients L_j:

$$\sum_j L_j\int_{\Delta\nu}W_{j,\nu}(-\mu_i)\frac{d\nu}{\Delta\nu}=I_{\bar{\nu}}\downarrow(Z_t,-\mu_i)-B_{\bar{\nu}}(T_c), \tag{27}$$

$$\sum_j L_j\int_{\Delta\nu}W_{j,\nu}(\mu_i)\exp(-k_{j,\nu}\tau_N)\frac{d\nu}{\Delta\nu}=I_{\bar{\nu}}\uparrow(Z_b,\mu_i)-B_{\bar{\nu}}(T_c). \tag{28}$$

After solving for L_j, the procedures for evaluating the radiation field in a cloudy atmosphere are complete, and we may therefore compute the upward and downward intensities at any given level in the atmosphere including the cloud layer. Without the cloud interference, the upward intensity at the top of the atmosphere is

$$I_{\bar{\nu}}\uparrow(\infty,\mu_i)=B_{\bar{\nu}}(T_0)\tau_{\bar{\nu}}(\infty,0)+\int_{\tau_{\bar{\nu}}(\infty,0)}^{1}B_{\bar{\nu}}[T(Z)]d\tau_{\bar{\nu}}(\infty,Z), \tag{29}$$

whereas in cloudy conditions, we have

$$I_{\bar{\nu}}\uparrow(\infty,\mu_i)=I_{\bar{\nu}}\uparrow(Z_t,\mu_i)\tau_{\bar{\nu}}(\infty,Z_t)+\int_{\tau_{\bar{\nu}}(\infty,Z_t)}^{1}B_{\bar{\nu}}[T(Z)]d\tau_{\bar{\nu}}(\infty,Z). \tag{30}$$

Here $I_{\bar{\nu}}\uparrow(Z_t,\mu_i)$ is to be evaluated from the previous section with the boundary conditions described above.

6. Results and discussions

Calculations of the transfer of infrared radiation through cloudy atmospheres were carried out for 16 discrete emergent angles. Since the variations of the radiation properties of cloud particles are comparatively small in the 800–1200 cm^{-1} window region, it was decided to divide this region into four spectral intervals. Optical parameters of cirrus were obtained by interpolating those tabulated in Table 1. The phase function of 11.5 μm was used for 800–900 cm^{-1}, while that of 10 μm was employed for the rest of the three spectral intervals. Resulting emergent intensities were averaged over the four spectral intervals. In the computations for the single scattering albedo, the effects of water vapor within clouds were taken into consideration, but its contribution is practically negligible. (Although in a strong band, the influence of water vapor is certainly significant.) Moreover, the downward intensity incident on the cloud top produced by the emission from small amount of water vapor is also negligibly small and may be ignored in the investigation of interaction of cirrus with the radiation field in the atmosphere. All the results presented below assume a number density of cloud particles of 0.05 cm^{-3} unless specified otherwise. It should be noted that the geometrical thickness as well as the number density are associated with the optical depth in a linear manner.

a. Radiative properties of cirrus

The transmitted and reflected intensities on the boundaries of cirrus with thicknesses of 1, 2 and 5 km in a tropical atmosphere are displayed in Fig. 3. The transmitted intensity for small cloud thicknesses reduces significantly when the effects of water vapor (mainly below the cloud) are considered. For thick cirrus, since the emission and multiple scattering of cloud particles dominate the radiation processes, gaseous contributions below the cloud appear to be unimportant. With water vapor included in radiation computations, the limb brightening for the reflected intensity decreases drastically. Initially, the emitted radiation from the earth surface is assumed to be isotropic, although such a radiation pattern is destroyed after undergoing gaseous absorption and the limb darkening effect becomes important. As a result, the radiation contribution from gases seems to introduce

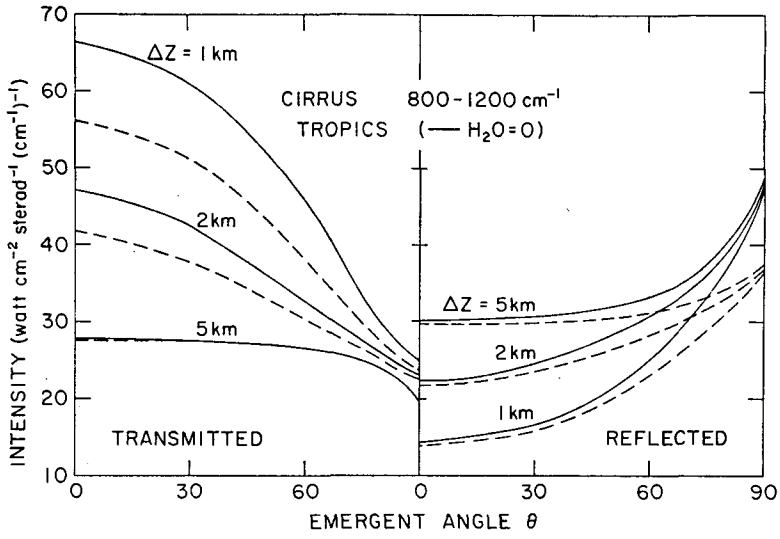

FIG. 3. Transmitted and reflected intensity as functions of the emergent angle (with respect to the zenith) on the boundaries of cirrus clouds for a model tropical atmosphere with (dashed lines) and without (solid lines) water vapor, for cloud thicknesses ΔZ of 1, 2 and 5 km. The intensity scale is in units of 10^{-7}.

less anisotropy for both the transmitted and reflected intensities from cloud layers. From this illustration, it is obvious that the water vapor below the cirrus cloud layers is an important factor in evaluating the radiative properties of thin cirrus. Fig. 4 shows similar computations for a mid-latitude winter atmosphere. Clearly, by changing from moist to dry atmospheric conditions, effects of water vapor decrease appreciably. For cirrus with thicknesses >5 km, the patterns of emergent intensities become nearly isotropic. This is because the mean optical depths of cirrus at the 800–1200 cm^{-1} window are $\gtrsim 7$, with the resulting emergent radiation depending mainly on the cloud temperature.

The flux transmission and reflection of cirrus in the window region shown in Fig. 5 are respectively defined as

$$\left.\begin{aligned}\tau_F &= F_{\tilde{\nu}}\uparrow(Z_t)/F_{\tilde{\nu}}\uparrow(Z_b)\\ \gamma_F &= F_{\tilde{\nu}}\downarrow(Z_b)/F_{\tilde{\nu}}\uparrow(Z_b)\end{aligned}\right\}, \tag{31}$$

where $F_{\tilde{\nu}}\uparrow$ and $F_{\tilde{\nu}}\downarrow$ stand for fluxes, and the flux emissivity

$$\epsilon_F = F_{\tilde{\nu}}/[\pi B_{\tilde{\nu}}(T_c)], \quad \text{when} \quad F_{\tilde{\nu}}\uparrow(Z_b)=0. \tag{32}$$

On the other hand, the transmission and reflection for the vertically emergent intensity (or radiance) from a

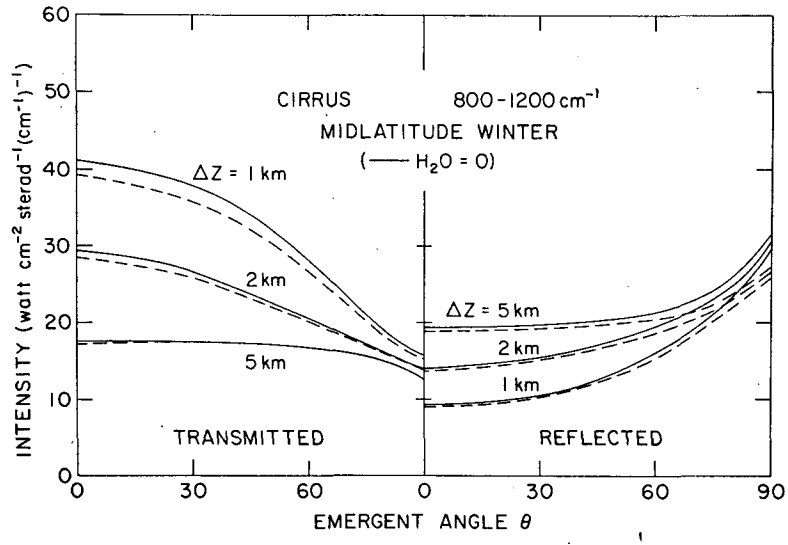

FIG. 4. As in Fig. 3, except for a mid-latitude winter atmosphere.

cloud layer are

$$\left.\begin{aligned}\tau &= I_{\tilde{\nu}}\uparrow(Z_t,1)/I_{\tilde{\nu}}\uparrow(Z_b,1)\\ \gamma &= I_{\tilde{\nu}}\downarrow(Z_b,1)/I_{\tilde{\nu}}\uparrow(Z_b,1)\end{aligned}\right\}, \tag{32}$$

and the intensity emissivity

$$\epsilon = I_{\tilde{\nu}}(1)/B_{\tilde{\nu}}(T_c), \quad \text{when} \quad I_{\tilde{\nu}}\uparrow(Z_b,1)=0. \tag{33}$$

In both cases, if no water vapor is considered, then $F_{\tilde{\nu}}\uparrow(Z_b)/\pi = I_{\tilde{\nu}}\uparrow(Z_b,1) = B_{\tilde{\nu}}(T_g)$. Since the emergent intensity is anisotropic, the transmission and reflection of flux should differ from those of intensity. The former quantities are important in the studies of radiation budget of the atmosphere, while the latter values are useful in remote sensing of the atmospheres from satellites.

Fig. 5 shows the intensity and flux transmission and reflection as functions of the cirrus thickness in the window region for the two model atmospheres. The intensity transmission defined in Eq. (32) is greater than the flux transmission with a value as high as 0.1 for thin cirrus arising from the strong forward scattering of cloud particles. On the contrary, the values of intensity reflection are less than those of flux reflection for all thicknesses, since the reflected intensity is stronger in the limb as we noted in the previous illustrations. These values seem to be independent of the

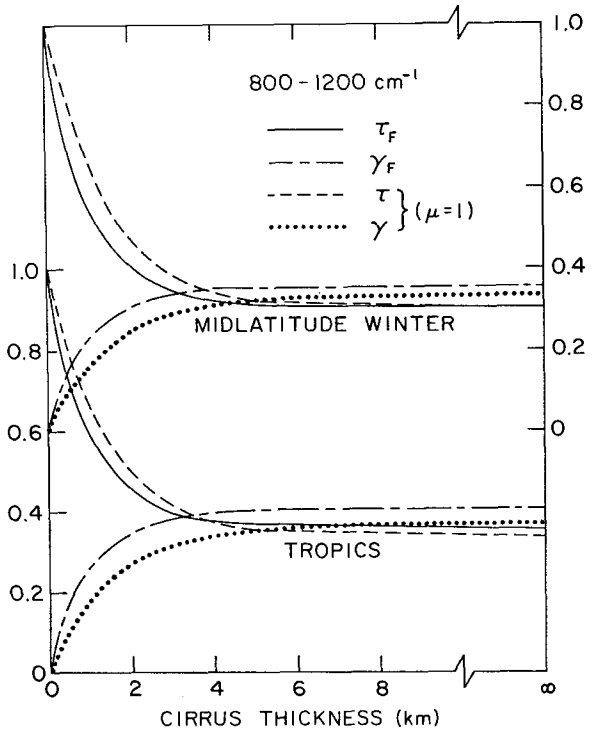

FIG. 5. Transmission and reflection for flux and the upwelling intensity (see text for definitions) as functions of the cloud thickness for two model atmospheres. The particle concentration employed is 0.05 cm^{-3}.

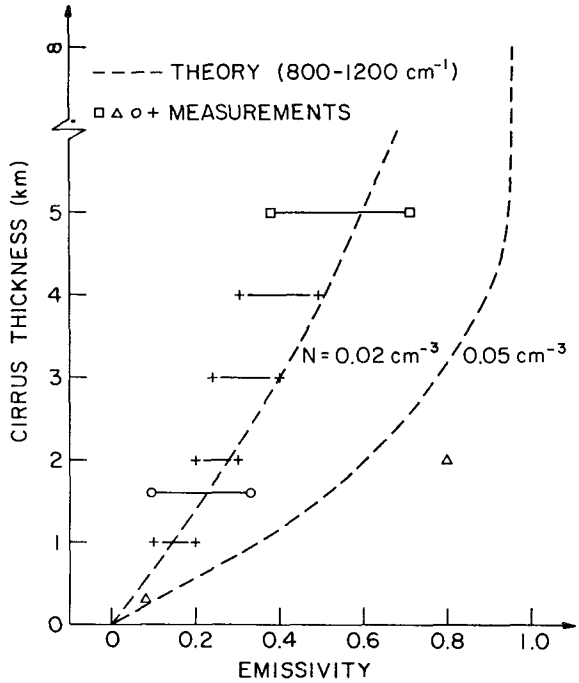

FIG. 6. Comparisons of the emissivity between theory (dashed lines) and observations. The symbols for the measured data are as follows: □ (Fritz and Rao, 1967), + (Kuhn and Weickmann, 1969), △ (Brewer and Houghton, 1956), and ○ (Platt and Gambling, 1971).

atmospheric conditions with few percent variations. For a 1-km cirrus (mean optical depth of about 1.4) in the tropics, the flux and intensity transmission are about 0.58 and 0.66, respectively. These values decrease to about 0.35 for cirrus clouds $\geqslant 5$ km thick which are essentially opaque to radiation beneath the cloud base. The value of 0.35 equals approximately the ratio of the brightness of the cloud to that of the ground.

Measurements of the emissivity of cirrus have been carried out by Kuhn and Weickmann (1969) who reported values of about 0.1–0.5 for clouds with thicknesses of 1–4 km. Fritz and Rao (1967) obtained values of 0.4–0.7 for a cirrus with a 5 km thickness. Brewer and Houghton (1956) indicated results of 0.08 and 0.8 for cirrus clouds whose thicknesses are 0.3 and 2 km, respectively. Recently, Platt and Gambling (1971) gave emissivities of 0.07–0.34 for 1.5–1.6 km thick cirrus. Since the radiometers mounted in the aircraft were either looking at the zenith or nadir direction the measured data refer to the intensity emissivity. All these values are displayed in Fig. 6. Clearly, the measured emissivity varies from one observation to another. Theoretical computations for the emissivity of numerous cloud thicknesses are made for particle concentrations N of 0.05 and 0.02 cm^{-3}. If the above emissivity data shown in Fig. 6 are reliable to within the instrumentation errors, then the concentration of ice crystals in cirrus must be on the order of 0.01–0.05

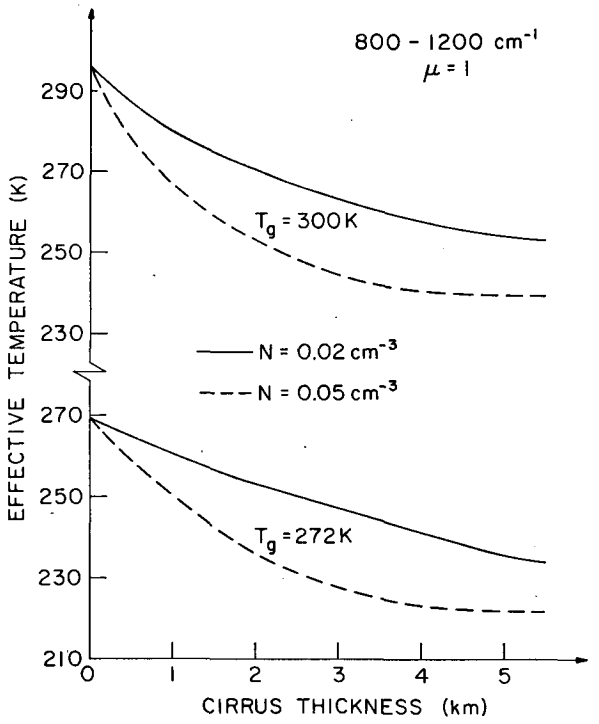

FIG. 7. Effective temperatures calculated from the upwelling intensity at the top of the atmosphere as functions of the cirrus thickness for two model atmospheres.

cm^{-3}. However, it is felt that Kuhn and Weickmann, and Fritz and Rao underestimated the emissivity of thick cirrus clouds. For a 4–5 km thick cirrus, the emissivity must be at least on the order of 0.7. At any rate, since the observations deviate greatly from each other, more comprehensive *in-situ* measurements of the radiative properties for cirrus clouds along with their composition (such as concentration and sizes) should be carried out in order that observation and theory can be compared in a more reliable manner.

On the basis of emissivity computations, a number of important points may be noted. First, the emissivity of a cloud with large optical depth appears to be independent of cloud temperature in the window region as indicated from the radiation computations. In addition, the emitted intensity from clouds indicates limb brightening, the degree of which becomes smaller with increasing thickness. This property has been noticed and discussed by Yamamoto *et al.* (1970). As a result of limb brightening, the flux emissivity is greater than the intensity emissivity when $\mu=1$. A difference of about 0.12 was found for a thickness of 1 km. Finally, the emissivity from a completely opaque cirrus never reaches 1 but rather a value of about 0.95. Thus, clouds can be considered as imperfect blackbodies.

For a fixed thickness, the emissivity depends basically upon two parameters, the particle concentration and the cloud temperature. The concentration greatly affects the optical depth of a cloud and consequently changes the radiative properties significantly, while the cloud temperature is the fundamental source of the emitted radiation. All the previous theoretical analyses assume isothermal cloud layers. However, the temperature gradient is certainly important in thick cirrus. Does it change the radiation pattern from a scattering particulate layer? It may not be very significant, but it should be investigated.

Finally, we would like to call attention to the transmission vs transmissivity and reflection vs reflectivity terms which have been used interchangeably for infared radiation in the literature. The transmissivity t and reflectivity r represent quantities without counting the cloud emission. These values can be evaluated by letting $B_{\tilde{\nu}}(T_c)=0$ in Eqs. (31) and (32). From the principle of the conservation of energy, we shall have $\epsilon+t+r=1$. Thus, if the reflectivity of clouds is negligibly small, we have $t\approx 1-\epsilon$. It should be noted that it is the transmission, reflection and emissivity (or emission) that are needed in the studies of radiation budget and in the sensing of the atmosphere.

b. Cirrus and remote sensing of surface temperatures

Owing to the relative transparency of the atmosphere in the window region, satellite radiance measurements in this channel give a first approximation to the effective temperature of the underlying surface such as ground, ocean and clouds. By correcting the effects of absorption due to intervening gases, more precise temperature of the emitting surface may be obtained. However, it has been noticed that cirrus clouds introduce serious problems in deriving the surface temperature. These troublesome problems in sensing of the surface temperatures may be classified into two categories: 1) the influence of a thin cirrus on the outgoing irradiance and the derived underlying surface temperature, and 2) the non-blackness of a relatively thick cirrus in estimating the cloud top temperature and therefore the height of the cloud top. The following discussion is an attempt to analyze these two problems.

Plots of the effective temperature computed from the upwelling intensity at the top of the atmosphere as functions of the thickness of cirrus clouds are shown in Fig. 7 for the tropical and mid-latitude winter atmospheres. The solid lines denote values for a particle concentration of 0.02 cm^{-3}, while the dotted lines are for a concentration of 0.05 cm^{-3}. Without cloud interference, the effective temperatures are about 294 and 271K for the moist and dry atmospheres, respectively. It is shown that the derived effective temperature strongly depends on the particle concentration and the cloud thickness, as well as the atmospheric conditions. Assuming a particle concentration of 0.05 cm^{-3}, the effective temperature decreases to about 235K (tropics), and 218.5K (mid-latitude winter) for cirrus clouds whose thicknesses are >5 km. Hence, cirrus clouds reduce the effective temperatures from about

0 to 60K. These values appear to be consistent with observations reported by Valovcin (1968) who indicated deviations of the effective temperature from 0 to 68K. Moreover, as mentioned earlier, the emissivity of an optically opaque cirrus is about 0.95, never approaching 1. Consequently, the estimated cloud temperature may be 1.5–2K lower than the actual values.

Having information on the transmission and emission characteristics of cirrus, it is possible to incorporate these two parameters in deriving the cloud and the underlying surface temperatures when cirrus is present in the field of view of the satellite radiometer. Since we are primarily interested in the upwelling radiation, all intensities referred to below are for $\mu=1$. We note that to a reasonable approximation water vapor above high cirrus can be neglected in the transfer calculations so that the observed radiance $I_{\tilde{\nu}}\uparrow(\infty)\approx I_{\tilde{\nu}}\uparrow(Z_t)$. Based upon the definition of the transmission function of cirrus discussed in the previous subsection, we have

$$I\uparrow(Z_b)\approx I_{\tilde{\nu}}\uparrow(\infty)/\tau^c(Z_t,Z_b). \tag{34}$$

Hence with a knowledge of the transmission function τ^c of cirrus, a reliable surface temperature may be estimated by taking the gaseous contribution below the cirrus into account. Here $I_{\tilde{\nu}}\uparrow(Z_b)$ represents the upward intensity at the base of a cloud layer. Further, the cloud temperature may be estimated from

$$B_{\tilde{\nu}}(T_c)\approx\frac{1}{\epsilon}[I_{\tilde{\nu}}\uparrow(\infty)-(1-\epsilon)I_{\tilde{\nu}}\uparrow(Z_b)], \tag{35}$$

where the second term on the right-hand side of Eq. (35) denotes the transmitted intensity arising from the component of the upward intensity just below the cloud. This value is to be evaluated from Eq. (34).

In view of the above analysis, it seems that both the cirrus cloud and the underlying surface temperatures may be obtained with reasonable accuracy provided that the transmission and emission properties of cirrus are known. Of course, the major problem would be then to classify cirrus clouds into finite numbers of categories so that their transmission and emission properties may be calculated once and for all. Further studies are needed to investigate the classification of cirrus clouds according to their radiative properties.

Acknowledgments. The author thanks Prof. R. G. Fleagle for reading the manuscript. The research was supported by the National Science Foundation under Grant GU-2655.

APPENDIX

Intensity Transmission and Emission from Cirrus Models

We have indicated in Section 3 that neither the "equivalent mass" nor the "equivalent cross section" of spheres serves as a good approximation for evaluating the single scattering properties of ice crystals. One may then ask how significant are these assumptions in the evaluation of the transmission and emission properties of cirrus, since the single scattering computations for spheres are well known from Mie theory. In order that a proper comparison can be made between the radiative properties obtained by the ice sphere model and those presented in this paper based on the ice cylinder model, the assumption of an "equivalent cross section" for spheres has to be made to match the optical depth calculated from the volume extinction cross section for cylinders. Table 2 shows such a comparison for values of the intensity transmission and emission for a tropical atmosphere. All the parameters were defined in Section 3. In order to obtain the "equivalent" volume extinction cross sections of spheres, the mode radius of about 65 μm is required. The single scattering albedo and the asymmetry factor for this cloud model in the window region are about 0.51 and 0.97, respectively, as compared with 0.53 and 0.85 for the ice cylinder model. It is clear that ice spheres absorb more infrared radiation and that the scattering is concentrated much more in the forward direction. In Table 2, the mean optical depth for a cirrus with a thickness of 1 km in the 800–1200 cm^{-1} window region is about 1.4. From these tabulations, it seems that the intensity transmission and emission evaluated from the assumption of an "equivalent cross section" for ice spheres have small variations as compared with those obtained from the ice cylinder model.

TABLE 2. Comparisons of the intensity transmission and emission calculated from the ice cylinder and ice sphere models.

ΔZ (km)	Cylinders* τ	Cylinders* ϵ	Spheres** τ	Spheres** ϵ
0.1	0.966	0.046	0.955	0.067
1	0.665	0.398	0.668	0.149
2	0.494	0.672	0.505	0.668
5	0.359	0.962	0.365	0.954

* Length 200 μm, radius 30 μm.
** Radius 65 μm.

REFERENCES

Bertie, J. E., H. J. Labbé and E. Whalley, 1969: Absorptivity of ice I in the range 4000-30 cm^{-1}. *J. Chem. Phys.*, **50**, 4501–4520.

Brewer, A. W., and J. T. Houghton, 1956: Some measurements of the flux of infrared radiation in the atmosphere. *Proc. Roy. Soc. London*, **20**, 167–175.

Chandrasekhar, S., 1950: *Radiative Transfer*. New York, Dover, 393 pp.

Elsasser, W. M., and M. F. Culbertson, 1960: Atmospheric radiation tables. *Meteor. Monogr.*, **4**, No. 23, 43 pp.

Fritz, S., and P. K. Rao, 1967: On the infrared transmission through cirrus clouds and the estimation of relative humidity. *J. Appl. Meteor.*, **6**, 1088–1096.

Goody, R. M., 1964: *Atmospheric Radiation*. Oxford, Clarendon Press, 436 pp.

Heymsfield, A. J., and R. G. Knollenberg, 1972: Properties of cirrus generating cells. *J. Atmos. Sci.*, **29**, 1358–1366.

Houghton, J. T., and G. E. Hunt, 1971: The detection of ice clouds from remote measurements of their emission in the far infrared. *Quart. J. Roy. Meteor. Soc.*, **96**, 1–17.

Huffman, P., and W. R. Thursby, Jr., 1969: Light scattering by ice crystals. *J. Atmos. Sci.*, **26**, 1073–1077.

Irvine, W. M., and J. B. Pollack, 1968: Infrared optical properties of water and ice spheres. *Icarus*, **8**, 324–366.

Kuhn, P. M., and H. K. Weickmann, 1969: High-altitude radiometric measurements of cirrus. *J. Appl. Meteor.*, **8**, 147–154.

Liou, K. N., 1972a: Electromagnetic scattering by arbitrarily oriented ice cylinders. *Appl. Opt.*, **11**, 667–674.

——, 1972b: Light scattering by ice clouds in the visible and infrared: A theoretical study. *J. Atmos. Sci.*, **29**, 524–536.

——, 1972c: Light scattering by cirrus clouds. *Preprints Conf. Atmospheric Radiation*, Fort Collins, Colo., Amer. Meteor. Soc., 121–127.

——, 1973a: Transfer of solar irradiance through cirrus cloud layers. *J. Geophys. Res.*, **78**, 1409–1418.

——, 1973b: A numerical experiment on Chandrasekhar's discrete-ordinate method for radiative transfer: Applications to cloudy and hazy atmospheres. *J. Atmos. Sci.*, **30**, 1303–1326.

——, and J. E. Hansen, 1971: Intensity and polarization for single scattering by polydisperse spheres: A comparison of ray-optics and Mie theory. *J. Atmos. Sci.*, **28**, 995–1004.

Maul, G. A., and M. Sidran, 1973: Atmospheric effects on ocean surface temperature sensing from the NOAA satellite scanning radiometer. *J. Geophys. Res.*, **78**, 1909–1916.

McClatchey, R. A., R. W. Fenn, J. E. Selby, F. F. Volz and J. S. Garing, 1971: Optical properties of the atmosphere. *Environ. Res. Papers*, No. 354, AFCRL, Bedford, Mass.

——, *et al.*, 1973: AFCRL atmospheric absorption line parameters compilation. *Environ. Res. Papers*, No. 434, AFCRL, Bedford, Mass.

Platt, C. M., and D. J. Gambling, 1971: Emissivity of high layer clouds by combined lidar and radiometric techniques. *Quart. J. Roy. Meteor. Soc.*, **97**, 322–325.

Roach, W. T., and R. M. Goody, 1958: Absorption and emission in the atmospheric window from 770 to 1250 cm^{-1}. *Quart. J. Roy. Meteor. Soc.*, **84**, 319–333.

Sanders, P., 1967: Aerial measurements of sea surface temperature in the infrared. *J. Geophys. Res.*, **72**, 4109–4117.

Schaaf, J. W., and D. Williams, 1973: Optical constants of ice in the infrared. *J. Opt. Soc. Amer.*, **63**, 726–732.

Valovcin, F. R., 1968: Infrared measurements of jet-stream cirrus. *J. Appl. Meteor.*, **7**, 817–826.

Wark, D. Q., G. Yamamoto and J. H. Lienesch, 1962: Methods of estimating infrared flux and surface temperature from meteorological satellites. *J. Atmos. Sci.*, **19**, 369–384.

Weickmann, H. K., 1949: Die Eispase in der Atmosphäre. *Ber. Deut. Wetterd.*, No. 6, 54 pp.

Yamamoto, G., M. Tanaka and S. Asano, 1970: Radiative transfer in the infrared region. *J. Atmos. Sci.*, **27**, 282–292.